Chiral Stereochemical Strategy for Antimicrobial Adhesion

Zixu Xie, Guofeng Li, and Xing Wang

Abstract Chiral stereochemical strategy (CSS) is a universal strategy that utilizes the "chiral taste" of microbes against their adhesion on chiral stereochemical surfaces. For the issue of interaction between microorganisms and material surface, molecular chirality or chiral stereochemistry plays a crucial role on modulating microbial behavior. The CSS thus is a soft management and control of microbes. It would not artificially promote the evolution of microbes, potentially preventing the formation of resistant organisms. This mini-review summarizes recent research on borneol-based chiral antimicrobial materials. According to the composition of the materials, we classified the borneol-based materials into synthetic polymers, natural polymers, and organic–inorganic hybrids. Their antimicrobial adhesion performance and the potential for biomedical applications were discussed. Due to the new concept of managing and controlling microbes, instead of killing microbes blindly, this review may catch special interest and inspire new opportunities in many medical fields and disciplines.

Keywords Chirality · Stereochemistry · Borneol · Antimicrobial · Adhesion

Introduction

Infections are the main causes of considerable morbidity and mortality to patients [1, 2], which is one of the most threatening problems worldwide. For example, implant failure due to infection is a thorny problem, which usually results in the removal of the implant [3–5]. The patients suffer tremendous pain and cost. Otherwise reports showed that hospital-acquired bacterial infections are mainly

Z. Xie · G. Li · X. Wang (✉)
Beijing Laboratory of Biomedical Materials, College of Life Science and Technology, Beijing University of Chemical Technology, Beijing, PR China
e-mail: wangxing@mail.buct.edu.cn

B. Li et al. (eds.), *Racing for the Surface*,
https://doi.org/10.1007/978-3-030-34475-7_19

attributed to the attachment of bacteria to surrounding objects, medical devices, and implants. Hospitals are not as safe as we think because of microbial distribution and contamination. Therefore, in order to reduce the risk of infections, researchers have been trying to explore efficient and safe antimicrobial materials. Until now, those developed antimicrobial materials have been fabricated mainly based on contact-killing mechanisms (such as quaternary ammoniums, quaternary phosphonium salts, and *N*-Halamines) [6–11] and release-killing mechanisms (such as antibiotic, silver or copper nanoparticles) [12–16]. However, the main problem now is the excessive use of antibiotics, which may lead to drug resistance of microbes [17–20]. Preventing bacterial resistance has become a hotspot for current antibacterial research. Thus, it is of great significance to develop new antimicrobial materials and strategies that are efficient, durable, and safe [21–23].

The chiral stereochemical strategy (CSS) is a novel strategy for antimicrobial studies, which is based on microbial recognition of the chiral stereochemical surface. A bacterium is a kind of microorganism who can distinguish different chiral surfaces [24] and have different adhesion and growth behavior on these surfaces [25]. According to studies, CSS for antimicrobial applications have been proposed [26, 27]. It is a broad-spectrum strategy that prevents bacterial and fungal cells from adhering to the material surfaces [26, 27], focusing on the initial stage of the microbial adhesion and contamination, allowing the microbes to autonomously leave the surface when they distinguish the chiral stereochemistry of the materials. The development of CSS has many potential advantages. First, it is a management and control of microbial behavior instead of killing the microbes, which does not artificially promote microbial evolution, prevent it from happening. Second, it is a broad-spectrum antimicrobial strategy against both bacteria (Gram-negative or Gram-positive) and fungi. Third, this strategy is applicable to a variety of materials, on the basis of versatile synthetic chemistry and surface modification. Finally, chiral units are mainly natural molecules, which are easily obtained in nature and cause little pollution to the natural environment. The chiral molecules are thus ideal candidates for antimicrobial materials.

In this review, we summarize recent studies about the applications of CSS in the field of synthetic polymers, natural polymers, and inorganic carbon materials. It is very exciting that all of these chiral stereochemical surfaces exhibit excellent antimicrobial adhesion activities.

Chiral Stereochemical Strategy

Chirality means that a molecule cannot overlap with its enantiomer, just like the left hand and the right hand mirrored each other cannot coincide. Chirality is ubiquitous in life. The interaction between biosystems and materials exhibits a high chiral preference. Therefore, CSS, based on the microbial recognition and follow-up response of the surface chiral stereochemistry, is a novel strategy for antimicrobial studies.

Chiral Effect on Cells

Selective interactions of cells on a chiral stereochemical surface was first found on calcium tartrate tetrahydrate crystals [28]. Epithelial A6 cells showed a strong preference of adhesion to the surfaces of (*R,R*) calcium tartrate tetrahydrate crystals, while few cells were found on (*S,S*) crystal surfaces (Fig. 1) [29]. The interaction between cells and the stereochemical structure of crystal surfaces indicated the specific chiral recognition of biosystems. From the macroscopic perspective, cells can distinguish chiral stereochemical signals of material surfaces. It is the first time we realized that this ability goes deep into the molecular level. This fact provided favorable evidence for the further study of cell behavior on chiral materials and interfaces.

Sun and his co-workers investigated the stereoselective behavior of immune cells on different *N*-Isobutyryl-L(D)-cysteine (NIBC) enantiomer-modified surfaces [30]. They used a mercapto self-assembled monolayer to simulate crystal surfaces. In a typical adhesion experiment, the number of macrophage cells adhering on the

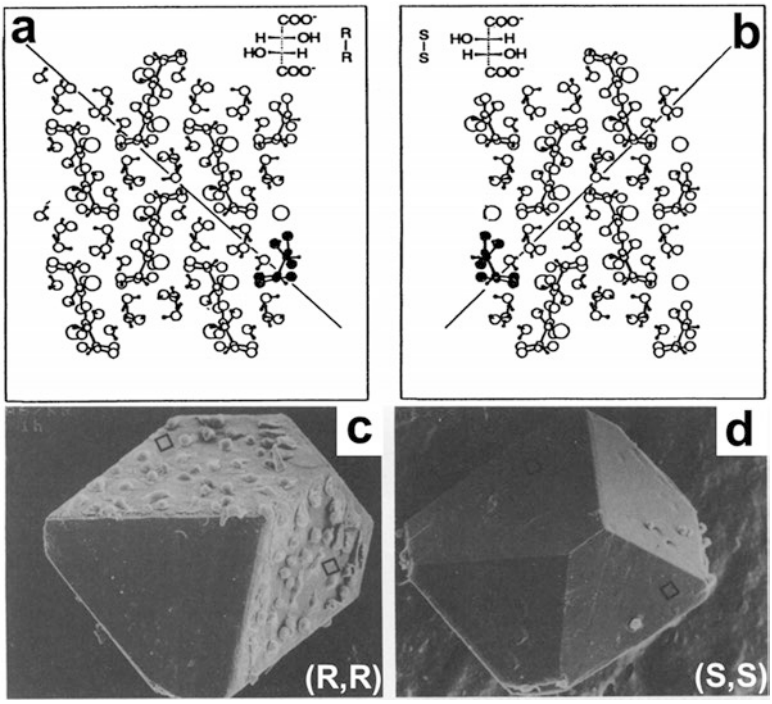

Fig. 1 (**a**, **b**) Computer graphic representation of the packing arrangement of (**a**) calcium *(R,R)*-tartrate tetrahydrate and (**b**) calcium *(S,S)*-tartrate tetrahydrate crystals viewed on the (100) plane. (**c**, **d**) Scanning electron micrographs of cultured Xenopus laevis kidney epithelial A6 cells plated on calcium tartrate tetrahydrate crystals. The short-term adhesive response (10 min) was shown for (**c**) the *(R,R)* form and (**d**) the *(S,S)* form [29]

L surface was much larger than that on the D surface. Moreover, macrophages on the L-NIBC surface showed a malformed morphology and highly spread status, whereas those on the D-NIBC surface remained a separate and round morphology. This phenomenon also happened in the adhesion experiment with neutrophils, further confirming the universality of cell behavior on chiral surfaces.

Besides, Luk et al. developed chiral antifouling materials inspired by the chiral recognition of biosystems [24, 31]. They found that mannitol terminated self-assembled monolayers (SAMs) decorated with various chiral enantiomer end-groups can oppose the conglutination of mammalian cells and bacteria on the surfaces. The adhesion of 3T3 fibroblast cells was limited on the D surface up to 19 days, while they were limited on the L surfaces for 13 days. Interestingly, the conglutination of cells on the surface that formed by the racemic mixture of the enantiomers was inhibited for 23 days, longer than either the L or D surface.

Compared to monolayer films, the polymer brush surface had a higher density of exposed chiral functional groups [32], which helped to enhance the chiral recognition of cells. Wang et al. investigated the adhesion of cells on the surface of chiral amino acid-based polymer brushes with different hydrophobic properties (Fig. 2). Cells were more willing to adhere to the hydrophobic surface; the adhesion number increased with increasing hydrophobicity of the polymer brushes. At the same time, they also found that chirality had the ability to regulate cell adhesion comparable to wettability properties. The concentration of cells on the L-poly(*N*-acryloyl-valine) (L-PV) film was evidently at a higher level than that on the D-poly(*N*-acryloyl-valine) (D-PV) film. For the quantitative analysis (Fig. 2a), the L-PV film also exhibited a much larger average area (*t*-test, $P < 0.01$) and higher I_f (fluorescent intensities) values (*t*-test, $P < 0.05$) than the D-PV film (Fig. 2b). These results emphasized the effect of chirality on cell adhesion [33]. More importantly, polymer brushes demonstrated attractive advantages such as the easy tailorability of chemical compositions, functions, and the precisely controlled surface properties with considerable bio-related applications.

Feng et al. discovered similar results for three-dimensional (3D) chiral nanofibers, which were prepared by 1,4-benzenedicarboxamide phenylalanine derivatives. It was revealed that left-handed helical nanofibers promoted cell adhesion and proliferation, while right-handed nanofibers inhibited these processes. These were attributed to the mediation of the stereospecific interaction between chiral nanofibers and fibronectin [35]. Furthermore, Liu et al. assembled chiral helical nanofibers by different chiral phenylalanine derivatives, and examined the effects of chiral molecules in these helical nanofibers on cells behavior. They found that there were clear-cut distinctions between the left- and right-handed nanofibers, even though both were formed by the same enantiomer phenylalanine derivatives. The results showed a rise in cell adhesion for the left-handed nanofibers formed by L-phenylalanine derivatives and a trifling impact on cell behavior on the corresponding right-handed nanofibers. By contrast, both left- and right-handed nanofibers formed by D-phenylalanine had minor and negative impacts on cell adhesion. The effects of single-handed molecules and helical nanofibers on cell adhesion are antagonistic [36]. This discovery indicated that the investigation on the chiral

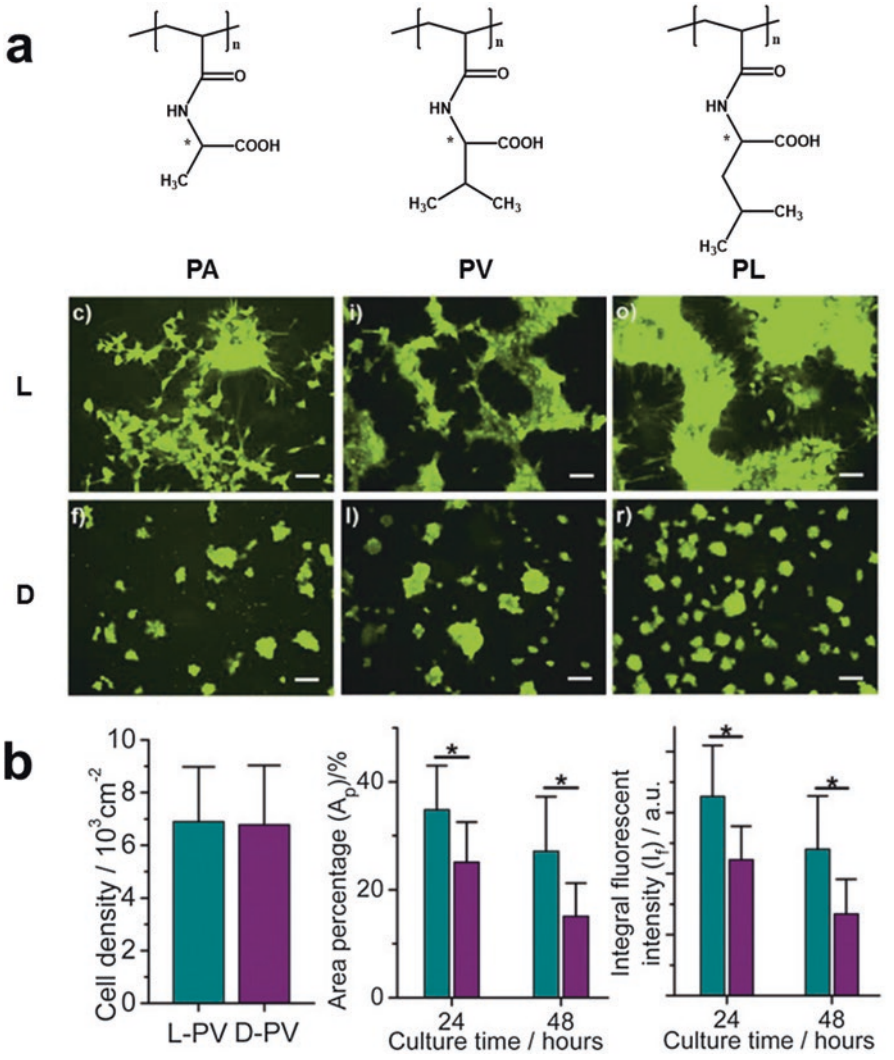

Fig. 2 (**a**) Structures of the chiral polymer and the corresponding typical fluorescent images of COS-7 cells incubated at different time periods on the chiral polymer brush films. (**b**) Cell counting results for 1 h of incubation (left); surface area ratios (Ar) occupied by cells after 24 and 48 h of incubation (middle); and integral fluorescent intensities (I_f, by arbitrary units (a.u.)) for the cell occupied areas on images after 24 and 48 h of incubation (right) [33, 34]

effect has gone deep into the relationship between designed molecular units and 3D assemblies.

Chirality adjusts not only the adhesion and growth of cells, but also their phagocytic behavior. Li et al. discovered that the chiral glutathione-coated CdTe quantum dots (GSH-QDs) exhibited differences in cytotoxicity, whereas L-GSH-QDs were

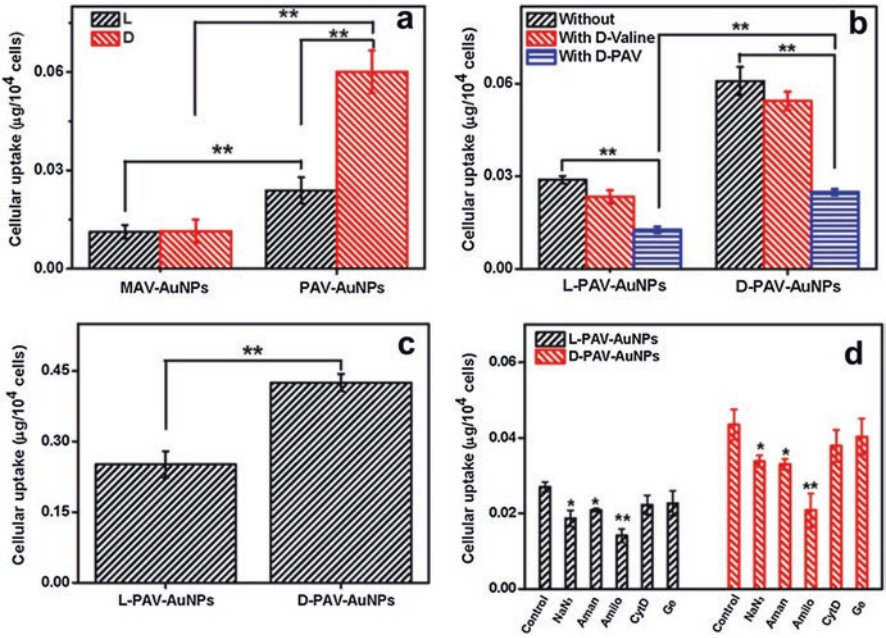

Fig. 3 Internalized amount by A549 cells at an Au concentration of 50 μg/mL. (**a**) L(D)-MAV-AuNPs and L(D)-PAV-AuNPs in 10% FBS/DMEM, (**b**) PAV-AuNPs pretreated with 1 mg/mL D-valine or D-PAV (M_w: 18,743 Da) in 10% FBS/DMEM, and (**c**) PAV-AuNPs in serum-free DMEM after co-incubation for 24 h. (**d**) Influence of pharmacological inhibitors on the uptake of L-PAV-AuNPs and D-PAV-AuNPs, respectively. The cells were cultured without or with pretreatment by amantadine-HCl (Aman, 1 mM, inhibitor of clathrin-mediated endocytosis), genistein (Ge, 100 μM, inhibitor of caveolae-mediated endocytosis), amiloride-HCl (Amilo, 2 mM, inhibitor of macropinocytosis), cytochalasin D (CytD, 10 μg/mL, inhibitor of cytoskeleton), NaN_3 (0.1% (w/v), inhibit energy-dependent process) for 1 h, and then cultured with PAV-AuNPs for another 4 h. ∗ and ∗∗ indicate significant difference at $p < 0.05$ and $p < 0.01$, respectively [38]

more cytotoxic than D-GSH-QDs due to the more cell uptake of L-GSH-QDs. Since the cytotoxicity of the QDs is associated with their ability to induce autophagy, this work exhibited a chiral dependent process [37].

After that, Gao et al. in 2016 found that the chirality of polymer-capped nanoparticles (NPs) could also affect cellular uptake. Interestingly, the internalization amount of D-poly(*N*-acryloyl-valine) gold nanoparticles (D-PAV-AuNPs) was significantly larger than that of the L-PAV-AuNPs (Fig. 3). This chirality-dependent cellular uptake might be ascribed to the stereoselective interaction between the cytomembrane and the chiral PAV molecule, which was deduced from the fact that L-phosphatidyl vesicles tend to interact with D-PAV molecules [38]. The chirality-dependent cellular uptake phenomenon was also improved by Kehr et al. They found that the cellular uptake amount of PMO-PL(D)L (Poly-L(D)-Lysine coated periodic mesoporous organosilica) varied by chirality [39]. Additionally, Gindi et al. found that C-6-glioma cells were able to adhere to the chiral penicillamine

functionalized zeolites, while the endothelial cells did not adhere at all. Therefore, they used an enantioselective L and D penicillamine functionalized zeolite (denoted as L-PEN-zeo and D-PEN-zeo) for the separation of C-6-glioma cells from primary endothelial cells [40].

All of these results demonstrated that the chiral recognition of cells on the chiral stereochemical surface is a universal phenomenon. Cells could distinguish chiral surfaces formed by small molecule modification, chiral polymer brushes, 3D chiral nanofibers, as well as chiral QDs and NPs. Cells can recognize different chiral interfaces for different responses, in which cells mainly showed a difference of adhesion at different chiral interfaces. Specifically, more cells preferred the L surfaces. This seems to be a ubiquitous phenomenon of cells.

Chiral Effect on Biomacromolecules

Biomacromolecules, such as proteins and DNA, were also found to recognize different chiral interfaces. In 2011, Wang et al. found that proteins could easily attach to the L surfaces of amino acid-based chiral polymer brushes [41]. Both bovine serum albumin (BSA, negatively charged) and gelatin (positively charged) were more inclined to adhere on the L-PV surface than on the D-PV surface (Fig. 4). Though electrostatic interactions affected the adhesion behavior of proteins on the surface to some extent, this electrostatic interaction was weaker compared with the stereoselective interaction between proteins and chiral surfaces. Some researchers also found that the chiral surface of NPs determined the adsorption orientation of proteins [42]. Chen et al. further confirmed this specific interaction by an adsorption test of BSA on the surface of chiral molecules-modified AuNPs. BSA adsorption orientation to chiral surfaces might result from the formation and location of salt bridges, which are affected greatly by the spatial distribution features of functional groups [43]. Moreover, the chirality of the surface could affect the morphology of proteins. For example, Aβ(1–40) preferred to form ring-like morphologies on

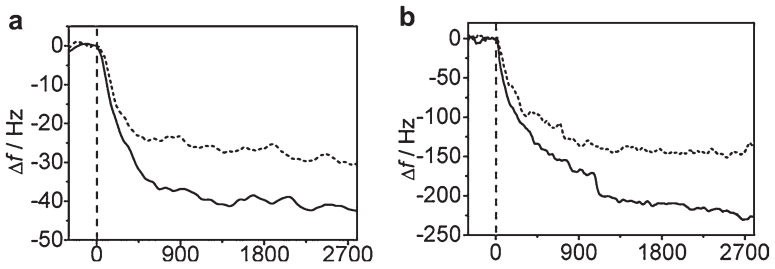

Fig. 4 Time-dependent curves of frequency change (Δf) in QCM experiments. (**a**) BSA adsorption and (**b**) gelatin adsorption on chiral polymer (L-PV and D-PV) brush films. Solid lines: L surfaces; dash lines: D surfaces [41]

L-*N*-isobutyryl cysteine (NIBC)-enantiomer-modified surfaces and rod-like morphologies on the D-NIBC-modified gold substrates [44].

Qing et al. studied the chiral effect at protein/graphene interfaces utilizing cysteine enantiomer-modified graphene oxide (Cys-GO) [45]. The result showed that the chirality of the Cys-GO surface greatly influenced protein folding, which would form amyloid aggregates. To be more specific, the R-Cys-GO inhibited the adsorption, nucleation, and fiber elongation processes of Aβ(1–40) and thus inhibited amyloid fibril formation on the surface to a large extent, while S-Cys-GO had the opposite effect. Surface chirality strongly influenced the conformational transition from an α-helix to β-sheet. More specifically, the S-Cys-GO accelerated this process, while the R-Cys-GO largely restrained this process. In addition, the adsorption of monomers and oligomers, and the subsequent fibrillation process were also influenced by the chirality of surfaces [45].

Gao et al. further proved that the chirality of NPs was one of the important factors, which affected the interaction of proteins and NPs. The adsorption of BSA on the L-PAV-AuNP surfaces was much higher than that on the D-PAV-AuNP surfaces, which was in consistence with the aforementioned conclusion. Moreover, when the BSA adhered on the L-PAV-AuNPs, it adopted an end-on configuration; however, when adsorbed on the D-PAV-AuNPs, the BSA displayed both side-on and end-on configurations (Fig. 5). The surface chiral modification of NPs could greatly influence the interaction between protein and NPs, and the subsequent protein adsorption and configuration on surfaces. Therefore, surface chirality could be an adjustable factor in the design of NPs for specific applications [46].

Chen et al. found that the L-Cys modified surfaces supported more serum protein adsorption than those on the D-Cys modified surfaces. More cells adhered on the

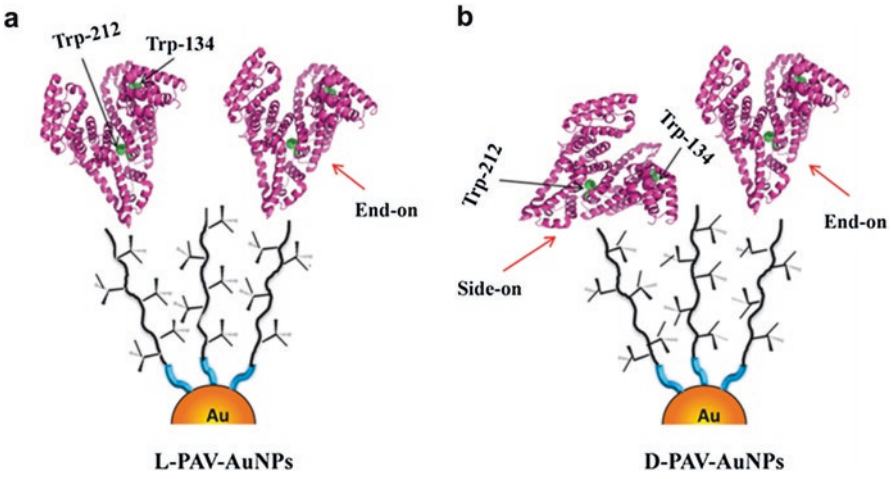

Fig. 5 Proposed binding geometries for BSA to (**a**) L-PAV-AuNPs and (**b**) D-PAV-AuNPs based on dynamic light scattering (DLS), fluorescence quenching, and isothermal titration calorimetry (ITC) measurements. NP and protein size are not drawn to scale

L-Cys modified surfaces under the serum-containing condition while under the serum-free condition, no significant differences were observed on both L and D surfaces. The results suggested that the differences of protein adsorption could be the reason for the preference of cells to attach to the L-Cys modified surfaces [47].

Tang et al. also found that DNA preferred to adhere on the surface modified with L-NIBC [48]. A full-sequence single-stranded DNA (ssDNA) from calf thymus tended to present a relaxed conformation on the L surfaces, while it folded on the D surface at a concentration of 50 μg/mL. When the concentration increased to 75 μg/mL, ssDNA preferred to exhibit a highly extended morphology (Fig 6). In addition, the quartz crystal microbalance (QCM) result showed that the quantity of the ssDNA on the L surface was much larger than that on the D surface (Fig. 6c, d). This stereoselective behavior of DNA was further confirmed by plasmid pcDNA3, which was a circular double-stranded DNA (ds-DNA). Similarly, the plasmid on the L surface exhibited a relaxed conformation, and its content was much larger than that on the D surface [49].

Proteins and DNA can recognize chiral systems and respond differently. This difference is not only reflected in the adhesion amount at different chiral interfaces, but also in the morphological conformation. Due to the effect of chirality, the conformation of protein could transfer from α-helix to β-sheet, while DNA could change from a relatively relaxed state to a rod-like folded state. These results provided clear evidence for the interaction between biomacromolecules and chiral systems, which may be an explanation of the difference of cell behavior on chiral surfaces.

To summarize, it is the nature of biosystems (cells, protein, DNA, etc.) that they can distinguish chiral stereochemistry structure and show different behavior. With this feature, chiral functional materials could be further designed and utilized, in particular, as antimicrobial materials in this review, where all of the abovementioned research can be regarded as the theoretical basis.

Antimicrobial Adhesion

Synthetic Polymers

Borneol molecules have been selected as ideal chiral units for antimicrobial applications. Borneol is a natural chiral drug that is presented in numerous medicinal plants. It has a hydrophobic molecular structure with four configurations, including endo-L-borneol, endo-D-borneol, and exo-isoborneol. They can be esterified into derivatives with increased activity compared to the parent borneol. Accordingly, our group has developed a series of chiral polyborneolacrylates (PBAs), including PLBA, PDBA, and PIBA depending on the three derivative enantiomers of BA [27].

In order to evaluate the antibacterial adhesion properties of PBAs, a “prison break” experiment was designed. The PBA rings were fixed into culture medium.

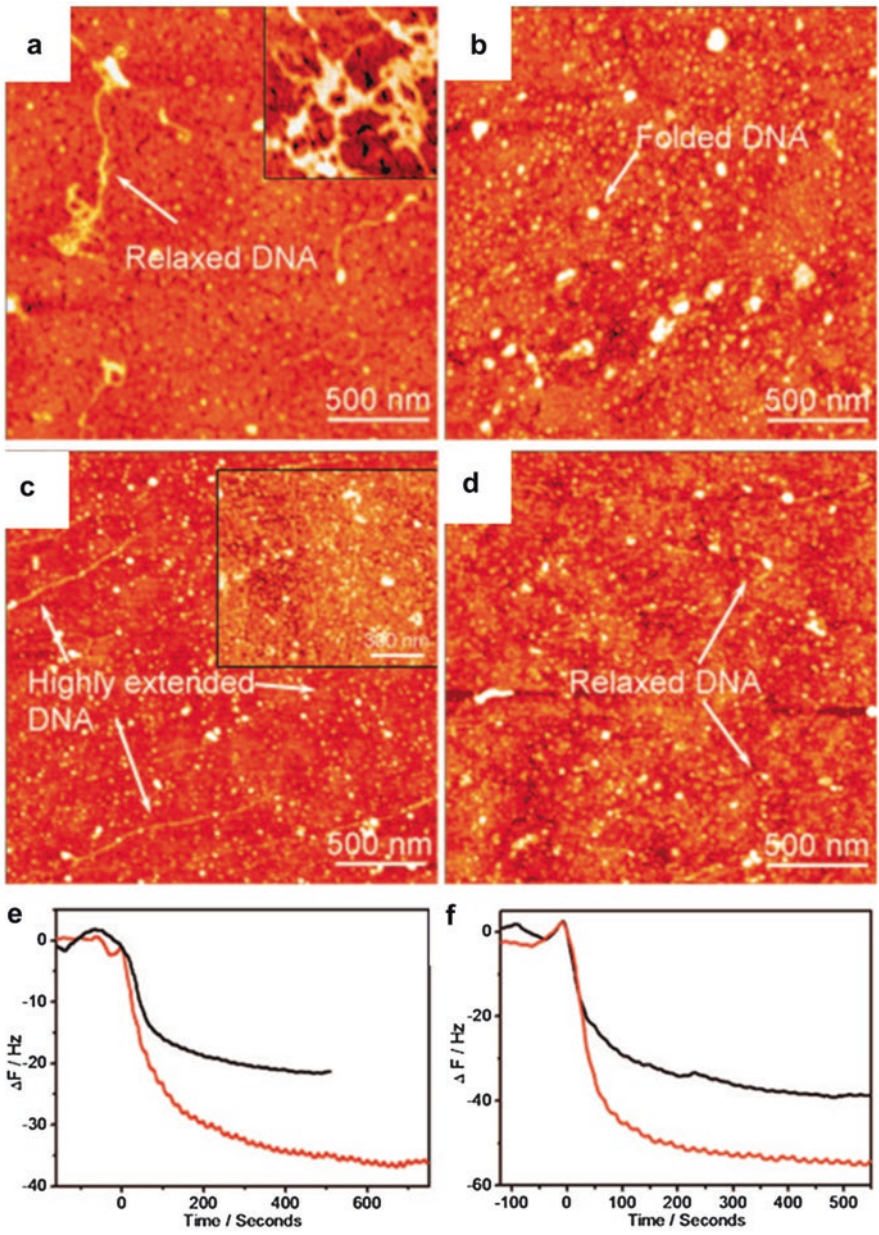

Fig. 6 Typical AFM (Atomic Force Microscope) images for DNA adsorption on L- (**a**, **c**) and D-NIBC (**b**, **d**) modified surface. DNA concentration: (**a** and **b**) 50 μg/mL; (**b** and **d**) 75 μg/mL. Inset in (**a**): Entangled DNA in another area. Inset in (**c**): DNA chains with another orientation and dense arrangement. (**e**, **f**) Time dependence of the QCM frequency shift of the D- (black) and L-NIBC (red) modified Au coated quartz-crystal resonator at DNA solutions with different concentrations. (**e**) 50 μg/mL; (**f**) 75 μg/mL. Experiment temperature: 25 °C [48]

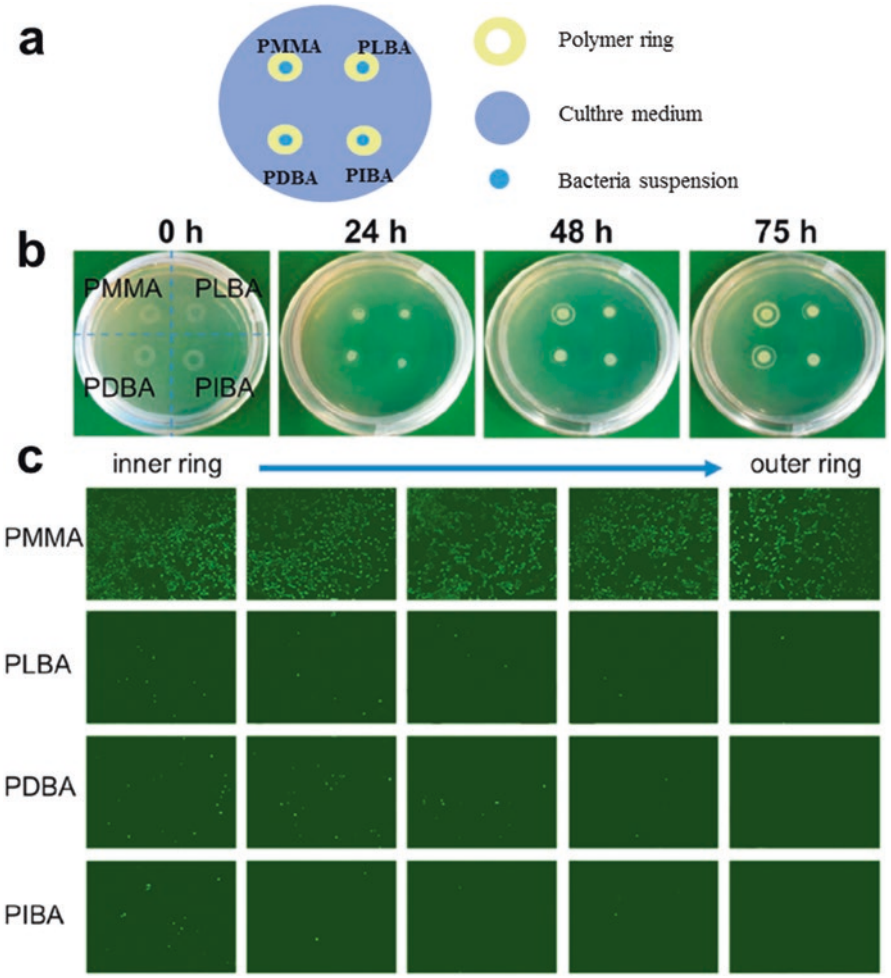

Fig. 7 (**a**) Schematic diagram of a "Prison Break" experiment for antibacterial adhesion assays of polymer films. (**b**) Effects on controlling the escape of *E. coli* from PMMA, PLBA, PDBA, and PIBA rings after different periods of incubation time. (**c**) Optical micrographs of *E. coli* adhered on the above polymers from the inner (left) to outer (right) edges of the rings after 60 h of incubation. The image size is approximately 897 μm^2 (34.5 μm × 26.0 μm) [27]

A bacterial suspension was placed onto the center of the circular ring and cultured for a period of time (Fig. 7).

A "Prison Break" experiment showed that bacteria easily broke the limitation of the poly(methyl methacrylate) (PMMA) control, while the PBAs showed excellent antibacterial adhesion properties. Scanning the polymer rings revealed that higher density of *E. coli* covered almost the entire surface of the PMMA from inside to outside. In contrary, only a few bacteria were found at the inner ring of the PBAs, while cells were barely observed on the outer ring of all the PBAs. These results

confirmed the antibacterial adhesion capability of the PBAs. The antibacterial capability of the PBA rings was caused by a biological surface recognition rather than the physical effect of blocking. Among the three enantiomers of the PBAs, the PLBA showed the best antibacterial adhesion property. Neither *E. coli* nor *S. aureus* could escape the PLBA ring after 75 h of incubation (Fig. 7b). This fact seems to be in violation of the previous finding, in which the L configuration surfaces may be good for the adhesion of biosystems. But, further investigation suggested that the camphane-type bicyclic structure of borneol had three chiral centers, located at C1, C2, and C4; the C2 chiral center in PLBA (*1S,2R,4S*-borneol pendants) corresponded to a D configuration, which usually provides surfaces with a cell or protein resistance capability. Thus, we envisioned that bacteria might mainly distinguish the chiral center at C2, rather than C1 or C4. Anyway, it was a successful antibacterial application of CSS.

Subsequently, the PLBA was used to modify the conventional biomedical polymer, PMMA, endowing PMMA with a surface stereochemistry property and enhancing its antibacterial adhesion capacity [50]. P(MMA-*co*-BA) was then synthesized via copolymerization of MMA and BA. By tuning the molar ratio of the MMA and BA, a series of P(MMA-*co*-BA)s were obtained. The modified "prison break" experiment (Fig. 8) showed that 10% of PBA (P_{10}) could give distinct antibacterial activity of the P(MMA-*co*-BA) copolymer. With increasing PBA content, the anti-adhesion activity of the P(MMA-*co*-BA) increased. P_{50} effectively prevented the adhesion and growth of *E. coli* on the copolymer surface and lasted for 120 h. In situ fluorescent live/dead staining showed that compared with P_0

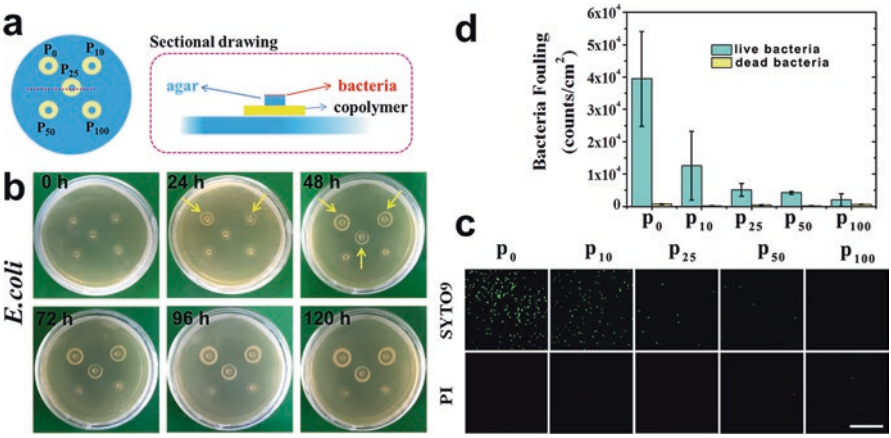

Fig. 8 (**a**) Schematic illustration of a modified "Prison Break" experiment for an antibacterial adhesion assay of polymer films. Controlling the escape of (**b**) *E. coli* and from *Px* films was recorded at the denoted periods (0, 24, 48, 72, 96, and 120 h). (**c**) Typical fluorescence microscopy images of attached *E. coli* from a suspension of 10^7 cells/mL after exposure to various films for 4 h. The live *E. coli* cells are stained green, while the dead cells are stained red. The scale bar in the image is 20 μm. (**d**) Quantitative results for bacterial adsorption on *Px* films. They were estimated using ImageJ software. Data values corresponded to mean ± SD ($n = 3$) [50]

(unmodified PMMA), the bacterial population reduced dramatically on the surfaces from P_{10} to P_{100}. Particularly, there was a 99.7% decrease in *E. coli* adhesion P_{100}. Meanwhile, only fragmentary dead bacteria could be found on all the surfaces, which was almost negligible. Thus, it not only testified that this kind of borneol-grafted copolymer had the capability of antibacterial adhesion but also confirmed that the activity was mainly due to initial sensing and subsequent selection of reversible bacterial attachment, relating interfacial stereochemistry rather than a normal mechanism of broken killing or virulence.

The PBAs showed excellent anti-adhesion ability against both Gram-positive and Gram-negative bacteria. Fungi, which are similar with mammalian cells, also have an inclination to different molecular chirality and tend to stay away from the stereochemical surface. Therefore, antifungal adhesion may be achieved on the PBA surfaces. To shed light on this issue, Xu et al. coated PBA polymers onto papers by a simple spraying method to impart the antifungal property of papers [51]. As shown in Fig. 9, the fungal growth started at the center of the plate, and then spread around to the edge of the material. After culturing for 8 days, fungal spores had covered almost the entire surface of the control paper, while the PBA-coated paper maintained a very clean surface, demonstrating that the PBA coating papers displayed an outstanding antifungal performance against *Aspergillus niger* (*A. niger*) and *Penicillium* sp. Unlike the traditional germicidal method, the PBA coating papers inhibited the attachment of fungal cells and the germination of fungal spores.

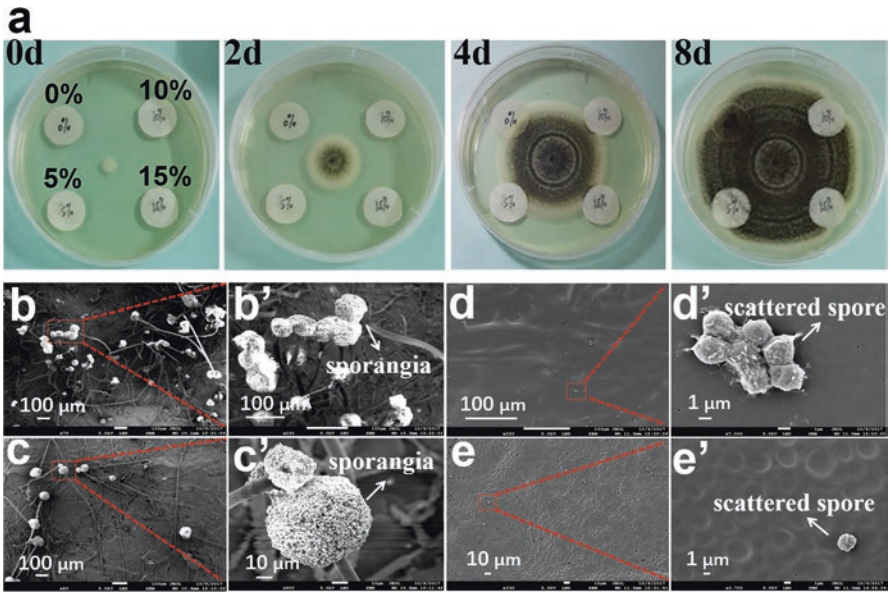

Fig. 9 (**a**) Antifungal effect of papers coated with 0 (left up), 5 (left down), 10 (right up), and 15% (right down) of PBA after incubating with *A. niger* for 8 days. (**b**–**e**) SEM images of *A. niger* cells on papers coated with 0 (**b**, **b**′), 5 (**c**, **c**′), 10 (**d**, **d**′) and 15% (**e**, **e**′) of PBA after incubating for 8 days. The images of (**b**′–**e**′) show zoomed-in views of areas in the corresponding images of (**b**–**e**) [51]

It was a remarkable breakthrough of CSS in the antifungal field, suggesting that CSS is a broad-spectrum antimicrobial strategy.

Utilizing the outstanding antibacterial adhesion ability of PBAs [27], Tan et al. introduced borneolacrylate into a diblock copolymer of poly[(N-3,4-dihydroxyphenethyl acrylamide)-*b*-(borneolacrylate)] (PDA-*b*-PBA) via reversible addition–fragmentation chain transfer (RAFT) polymerization. The PDA-*b*-PBA was endowed with both an excellent adhesive property and antibacterial ability. The PDA-*b*-PBA coating showed a good broad-spectrum antibacterial performance with inhibition rates of 92.7% and 81.3% for *E. coli* and *S. aureus*, respectively. In addition, the PDA-*b*-PBA coating could be applied in antibacterial textiles due to its easy fabrication on cotton fabrics and commercial gauze (see the plate count results in Fig. 10) [52]. Moreover, Wu et al. developed a waterborne polyurethane functionalized with IBA side group (IWPU). The introduction of IBA gave IWPU a unique chiral feature and good antibacterial adhesion activity against *E. coli* and *S. aureus*. The antibacterial activity was positively correlated with IBA side group content. When the content of the IBA side groups reached 25%, the IWPU exhibited a very effective resistance to bacterial adhesion [53].

Natural Polymers

Natural polymers, cellulose in particular, had been employed in textiles [54], food packaging [55, 56], the medical field [57–59], and the environmental domain [60, 61]. One of the main problems that hinder their applications is that these materials

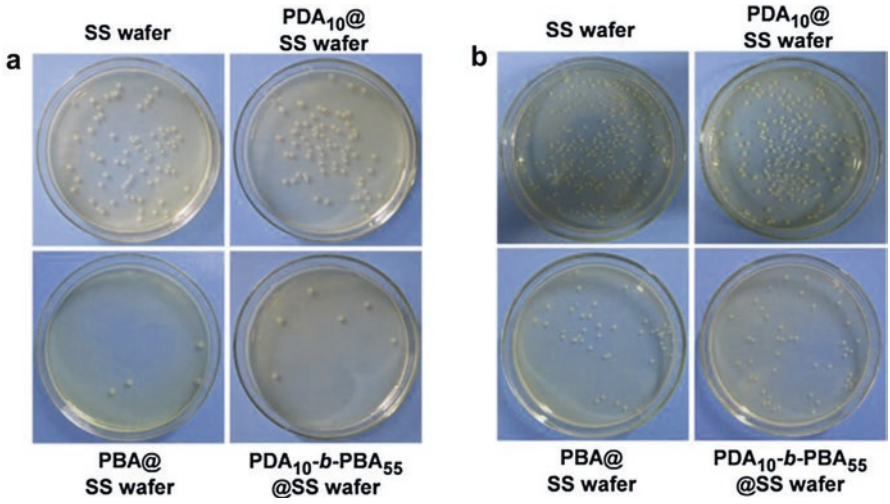

Fig. 10 The photos of (**a**) *E. coli* colonies and (**b**) *S. aureus* colonies in plate count experiments [52]

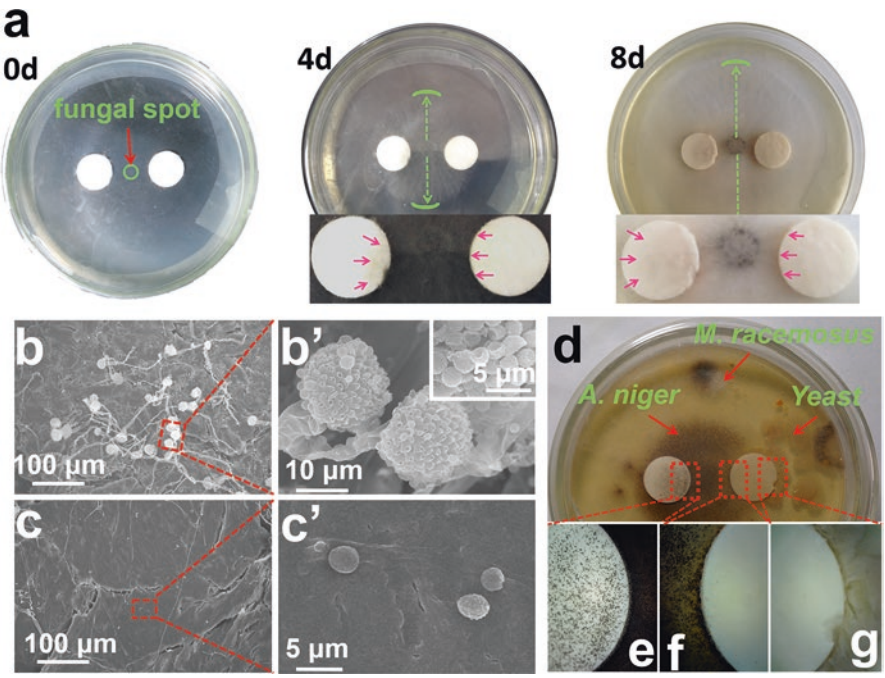

Fig. 11 (**a**) Study of the antifungal adhesion activity of cellulose (left) and BGC (right) pellets, by culturing *M. racemosus* in the central location of the solid medium, in the same plate for different periods of time. The results of 0, 4, and 8 days are shown here. The insets exhibit an enlarged image. Pink arrow: the growth frontier of *M. racemosus* on the pellets. Green circle: the range of the inoculated *M. racemosus* spot. Green arc: the growth range of *M. racemosus*; (**b**, **c**) SEM images of the antifungal adhesion results for the cellulose (**b**, **b**′) surface and the BGC (**c**, **c**′) surface. By comparison, distinct antifungal adhesion inhibition could be found after grafting borneol molecules onto cellulose; (**d**) antifungal adhesion activity of pellets of cellulose (left) and BGC (right) by culturing *A. niger* for 8 days. The operation was carried out in ambient conditions, thus, *M. racemosus* and yeast strains were also found. Optical micrographs showed that the fungal cells adhered to the cellulose pellet (inset **e**) and stopped adhering to the BGC pellet (inset **f** and **g**) [26]

do not have antimicrobial properties. Thus, to endow these natural materials with broad-spectrum antimicrobial properties, borneol was used to modify the surface of the materials and enabled them with antimicrobial properties.

Shi et al. synthesized borneol-grafted cellulose (BGC) by covalently tethering L-borneol to cellulose [26]. The BGC showed effective antifungal adhesion activity against *M. racemosus* and *A. niger*. Its surface kept a relative cleanliness even though the evaluation time was up to 8 days. By contrast, the control cellulose surface was almost covered with fungal cells (Fig. 11a, e). Scanning electron microscope (SEM) images showed that a large number of grown sporangia and hypha were found on the cellulose surface and lively germination of spores was exhibited therein. While on the BGC surface (Fig. 11a, f), only a few hyphae could be observed near the boundary and the serendipitous spores stayed near the

hypha presenting a whole sphericity, indicating growth inhibition of spores on the BGC surface. Then, a special antimicrobial evaluation was carried out in an open environment. A large number of *M. racemosus*, *A. niger*, and yeast grew in the medium and climbed on cellulose surface (Fig. 11g), while no cells tended to adhere on the surface of the BGC pellet, revealing its great application potential. Above all, these phenomena demonstrated the success of the cellulose modification and the high antifungal power of the grafted borneol molecules.

Xu et al. developed a borneol-decorated cotton textile (BDCT) through coupling of borneol 4-formylbenzoate molecules onto the amino-modified CT. The new functionalized CT exhibited prominent antifungal adhesion properties against *M. racemosus* and *A. niger* for more than 30 days (Fig. 12a). It also exhibited broad-spectrum antibacterial activities against *E. coli*, *P. aeruginosa*, *S. aureus*, and *S. epidermidis* (Fig. 12c). The antimicrobial adhesion rates were all above 93%

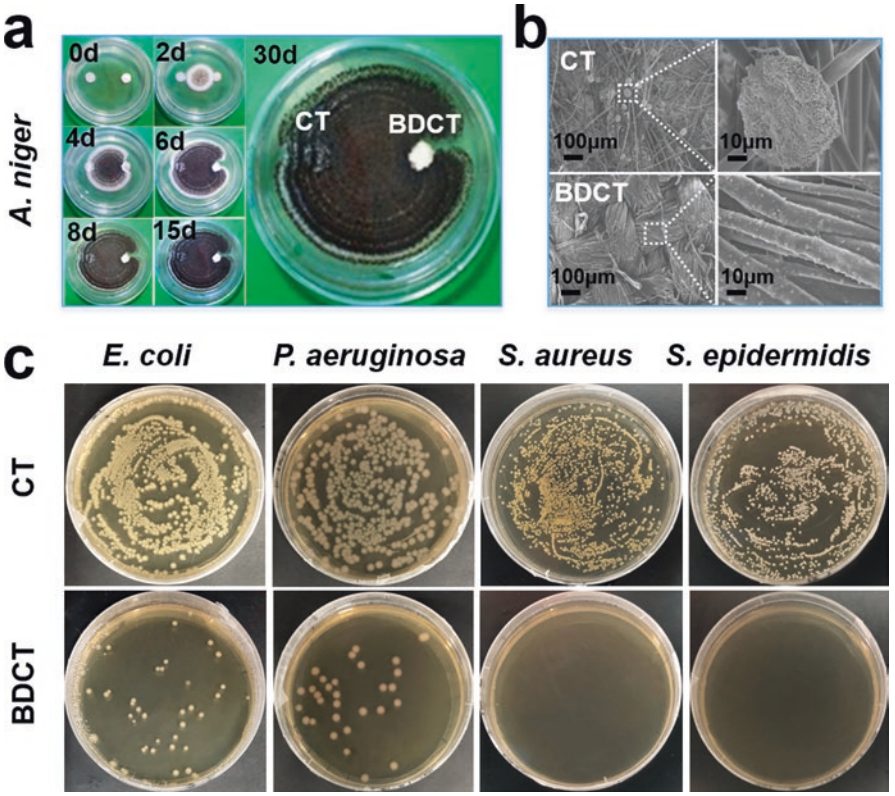

Fig. 12 (**a**) Effect of antifungal adhesion on raw CT (left), and BDCT (right) by culturing *A. niger* in the center location of solid medium, in the same plate for different time periods (0, 2, 4, 6, 8, 15, and 30 days). (**b**) SEM images of antifungal adhesion results on raw CT and BDCT surfaces. Left are images at low magnifications; right are images at high magnifications. (**c**) Antibacterial activities of raw control CT and BDCT against *E. coli*, *P. aeruginosa*, *S. aureus*, and *S. epidermidis* [62]

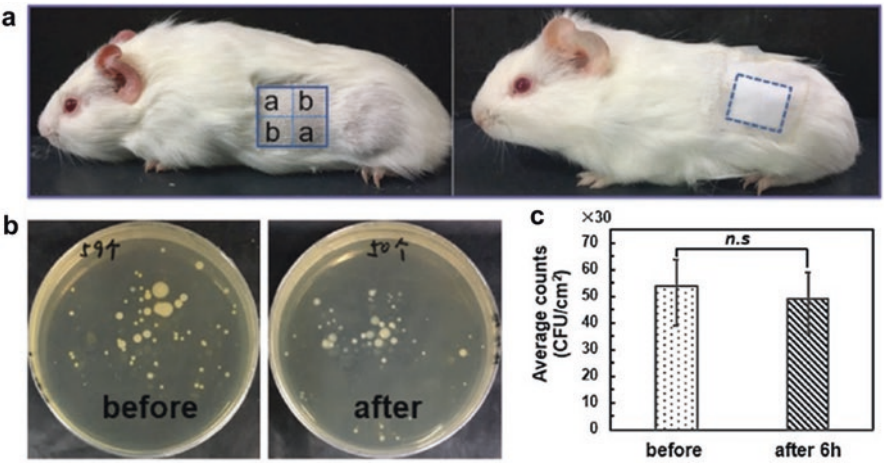

Fig. 13 (**a**) Model of skin flora test: Guinea pig in the left picture showed the application of the site to cover the sample (marked with blue line). The region "a" was the area bacteria were taken from before coating samples. The region "b" was the area bacteria were taken from after coating the samples. The right picture shows a guinea pig in contact with the BDCT. (**b**) The culturing results of bacterial flora from the guinea pig skin before and after applying BDCT. (**c**) Average of total germ count before and after the application of BDCT [62]

after 50 times of an accelerated laundering test. The antimicrobial mechanism was mainly due to the special stereochemistry of L-borneol instead of hydrophobicity. Therefore, it was different from a traditional bacterial-killing strategy, which was conducive to maintain skin microecological balance and did not damage the skin flora protection barrier. As shown in Fig. 13, the number and species of a guinea pig's skin flora remained almost the same after contacting with the BDCT for 6 h. Besides, it showed no skin stimulation due to no antibacterial release. For the perspective of application, the BDCT is meeting the frontier of antimicrobial CT, in which beneficial microbes should live in harmony with humans, as well as protecting us from potentially harmful microorganisms. Thus, the BDCT-like materials could be utilized in many industries such as clothing, medical, food packaging, as well as environmental domains to control the spread of infectious microorganisms.

Chitosan is another natural material that is derived from the deacetylation of chitin [63] and known as the only pseudonatural cationic polymer [64]. As a promising biomaterial, chitosan has the advantages of good biocompatibility, high safety, and excellent film-forming ability [65], and is widely used in pharmaceutical [66–68], food [69, 70], textile [71, 72], cosmetics industries [73, 74], etc. Furthermore, the broad-spectrum antibacterial property of chitosan [75–78] makes it an ideal antibacterial model. However, studies have shown that the good antibacterial properties of chitosan can only be acted in the aqueous solution state, while in the solid state, the antibacterial property of chitosan drops sharply [79]. Therefore, to solve this

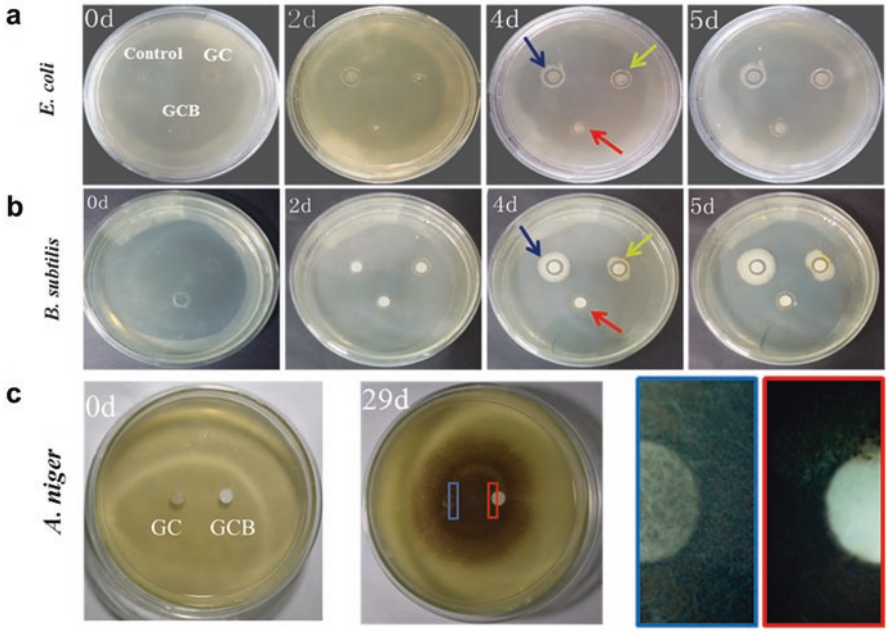

Fig. 14 (**a**, **b**) Effects on controlling the escape of *E. coli* (**a**) and *B. subtilis* (**b**) from control, GC, and GCB rings after different periods of incubation time. (**c**) Study of the antifungal adhesion activity of GC (left) and GCB (right) pellets, by culturing *A. niger* for 0 and 29 days. The red and blue boxes correspond to the adhesion of fungi on GC and GCB materials [85]

problem, the surface modification of chitosan is desirable. It mainly focuses on the introduction of silver [80, 81], quaternary ammonium salt [82, 83], antibacterial peptides [84], etc. to chitosan. However, all those efforts are traditional bacteria-killing strategies, either harmful pathogen or beneficial flora.

Therefore, our group prepared a glycol–chitosan/borneol (GCB) composite by a facile Schiff base reaction. The specific stereochemistry of the GCB impacted the microbial sensing system to achieve an antimicrobial purpose. The antibacterial "Prison Break" experiment showed that bacteria were confined within the GCB ring for at least 5 days (Fig. 14a, b). The antifungal experiment also confirmed that the GCB surface possessed long-term antifungal properties and was kept clean after 29 days of incubation, while the control tablet was covered with dense fungi (Fig. 14c). The skin flora evaluation was also carried out by the same animal model (Fig. 13a), where the silver NPs (AgNPs) modified material was used as a control group. On the skin of a healthy guinea pig, there was a lot of yellow flocculent *Kurthia* and white *Acinetobacter*, which were classified as cross-flora and symbiotic flora, respectively. After contacting with the GCB for 6 h in a preliminary test, the species and number of microorganisms were not reduced [85]. However, the number of microorganisms in that AgNPs material group decreased evidently. The results indicated that GCB was friendly to the intrinsic skin flora.

Inorganic Carbon Materials

Graphene and its derivatives have been widely used as bactericidal agents [86–88]. Their antibacterial mechanisms mainly include nanoknives, oxidative stress, and membrane wrapping or trapping. However, most of these mechanisms are available when the graphene-based materials (GMs) are dispersed in solution, while those are not feasible for on-surface graphene oxide (GO) or reduced GO (RGO). The solid graphene-based materials did not show any antifungal properties. Therefore, our group combined borneol and GO, endowed graphene-based material with antifungal performance, and further demonstrated its antifungal mechanism [89].

A GO–borneol (GOB) composite was synthesized by esterification of borneol with thiomalic acid-modified GO sheets. The landing test (Fig. 15a) showed that the GOB tablet was the only one that no *M. racemosus* cells adhered or grew on it, while the other tablets failed to resist the adhesion of *M. racemosus* (Fig. 15b). A large number of *M. racemosus* cells could be seen to gathering in the frontier of the tablets of GO, RGO, and GOC, and their edges were ambiguous (Fig. 15c). These results were in agreement with the previous study that neither solid GO nor RGO could resist fungal adhesion [90]. In contrast, the GOB exhibited outstanding antifungal activity. *M. racemosus* grew outside the GOB tablet. Only a few individual cells scattered in the edge of the GOB. Previous studies [87, 91] revealed that the needlelike nanostructure of GO (like a nanoknife) could pierce the bacteria cell membrane and led to the efflux of cell contents. This effect on fungi, however, was very weak because the fungal hyphae were too large to be damaged by these nanostructures of the solid GO (Fig. 15d). By contrast, the chiral borneol molecules in the GOB could be the key sensors to avoid the contamination of fungi. Therefore, this was a successful combination of inorganic material and the CSS.

Conclusions and Perspectives

In summary, biosystems have intrinsic chiral preference, in other words, the chiral taste is a nature of biosystems. Cells or microbes, proteins or DNA all exhibit significant differences in behavior on chiral stereochemical surfaces. With this feature, multi types of chiral functional materials could be designed and further tailored for a particular purpose. Until now, we know that it could be used for cell separation [40, 93], biosensing system [94, 95], pharmaceutical industries [96–98], and antimicrobial materials of course.

On the basis of this understanding, we utilized CSS to develop a series of borneol-based chiral stereochemical materials, including synthetic polymers, natural polymers, and organic–inorganic hybrids. The CSS is a ubiquitous antimicrobial adhesion strategy that is based on the reversible recognition and sensing effect of the microbes on a material interface, focusing on the initial stage of bacterial contamination, allowing the microbes to autonomously leave the surface when they

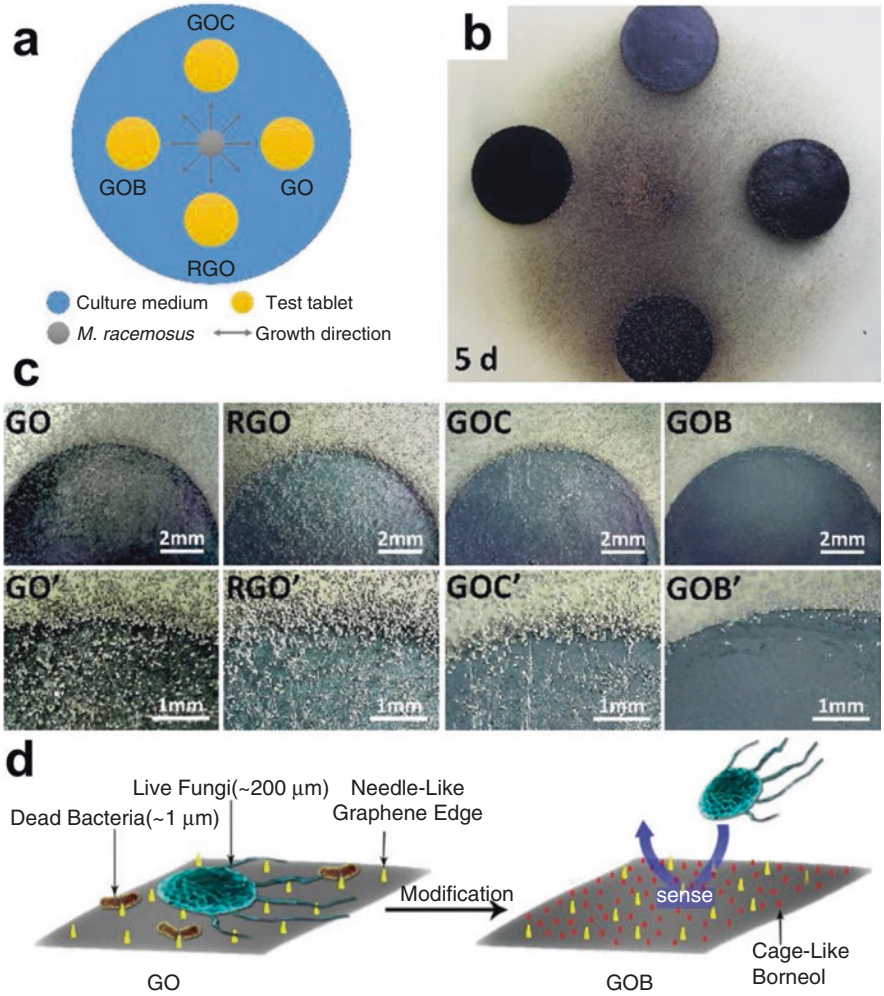

Fig. 15 Antifungal activity of GO, RGO, GOC, and GOB. (**a**) Schematic representation of the antifungal model. (**b**) Optical photograph of antifungal activity of the samples by culturing *M. racemosus* for 5 days. (**c**) Enlarged images of (**b**). (**d**) Schematic representation of the antifungal mechanism of the GOB. Fungi are large enough that they can weaken the damage caused by the needlelike nanostructure of the solid GO, while fungi avoid adhering on the surface of the GOB by sensing the carbon stereochemistry of the GOB [92]

distinguish the stereochemical signals of the materials. Therefore, the obtained borneol-based materials possessed broad-spectrum (Gram-negative bacteria, Gram-positive bacteria and various fungi), safe (antimicrobial adhesion other than killing or virulence) and long-term (lasting for more than 1 month) antimicrobial activities.

Although great achievements had been made in the application of CSS, the study is still in its infancy, and a lot of challenges remain to be solved. In our opinion,

the focus of future work will be tilted toward three aspects. The first is to find out the underlying antimicrobial adhesion mechanism since it has not been completely understood. Currently, it was confirmed that the antimicrobial activities of borneol-based materials were mainly due to initial sensing and subsequent selection of reversible microbial attachment, relating interfacial stereochemistry of borneol-based materials, rather than the normal mechanism of killing or virulence. However, it is still unclear what kind of bacterial sensory system is used to identify the chiral surface, and that will be the challenge for deeper research. The second aspect is finding a more flexible type of applicable chiral units. Although there is an infinity of possible chiral molecules, not all of them are capable for antimicrobial applications. In addition, CSS of the borneol-based materials is mainly a characteristic of antimicrobial adhesion, which does not artificially promote the evolution of microbes theoretically, but, detailed verification tests are still lacking. Therefore, the key work of the future is to determine if it will lead to the formation of resistance.

The CSS is, in fact, a management and control of microbial behavior. It will not take the initiative to attack microbes, which will be one trend of other antimicrobial material developed. Currently, this new antimicrobial concept can achieve a harmonic antimicrobial model, protecting us from potentially harmful microorganisms without harming the skin flora of human beings. This harmonic thinking is good agreement with the Chinese traditional military strategies and tactics, The Art of War, written by Sun Tzu: *Hence to fight and conquer in all your battles is not supreme excellence; supreme excellence consists in breaking the enemy's resistance without fighting. The highest form of generalship is to balk the enemy's plans; the next best is to prevent the junction of the enemy's forces; the next in order is to attack the enemy's army in the field, and the worst policy of all is to besiege walled cities.* Hence, a microbe's reversible adhesion on material surfaces in the initial stage can be seen as the microbe's plan; while the formed biofilm looks more like the walled city. Although there are limitations to kill microbes, antimicrobial adhesion is our option to some extent. What we will see in the future is, we are confident, a continuation of that harmonic trend, to solve a great variety of problems in many diverse scenarios.

Acknowledgments The authors thank the National Natural Science Foundation of China (21574008) and the Fundamental Research Funds for the Central Universities (BHYC1705B) for their financial support.

References

1. Rutledge-Taylor K, Matlow A, Gravel D, Embree J, Saux NL, Johnston L, Suh K, Embil J, Henderson E, Control, M. J. J. A. A. J. o. I (2012) A point prevalence survey of health care-associated infections in Canadian pediatric inpatients. Am J Infect Control 40(6):491–496
2. Allegranzi BJL (2011) Burden of endemic health-care-associated infection in developing countries: systematic review and meta-analysis. Lancet 377(9761):228–241

3. Zhao L, Chu PK, Zhang Y, Wu Z (2010) Antibacterial coatings on titanium implants. J Biomed Mater Res Pt B Appl Biomater 91B(1):470–480
4. Szaraniec B, Pielichowska K, Pac E, Menaszek E (2018) Multifunctional polymer coatings for titanium implants. Korean J Couns Psychother 93:950–957
5. Peng F, Wang D, Zhang D, Cao H, Liu X (2018) The prospect of layered double hydroxide as bone implants: a study of mechanical properties, cytocompatibility and antibacterial activity. Appl Clay Sci 165:179–187
6. Krishnamoorthy M, Hakobyan S, Ramstedt M, Gautrot JE (2014) Surface-initiated polymer brushes in the biomedical field: applications in membrane science, biosensing, cell culture, regenerative medicine and antibacterial coatings. Chem Rev 114(21):10976
7. Agnihotri S, Mukherji S, Mukherji S (2013) Immobilized silver nanoparticles enhance contact killing and show highest efficacy: elucidation of the mechanism of bactericidal action of silver. Nanoscale 5(16):7328–7340
8. Vincent M, Duval RE, Hartemann P, Engels-Deutsch M (2018) Contact killing and antimicrobial properties of copper. J Appl Microbiol 124(5):1032–1046
9. Dong A, Wang Y-J, Gao Y, Gao T, Gao G (2017) Chemical insights into antibacterial N-Halamines. Chem Rev 117(6):4806–4862
10. Makvandi P, Jamaledin R, Jabbari M, Nikfarjam N, Borzacchiello AJDM (2018) Antibacterial quaternary ammonium compounds in dental materials: a systematic review. Dent Mater 34(6):851–867
11. Kenawy ER, Abdel-Hay FI, El-Shanshoury AERR, El-Newehy MH (2002) Biologically active polymers. V. Synthesis and antimicrobial activity of modified poly(glycidyl methacrylate-co-2-hydroxyethyl methacrylate) derivatives with quaternary ammonium and phosphonium salts. J Polym Sci A Polym Chem 40(14):2384–2393
12. Li Z, Lee D, Sheng X, Cohen RE, Rubner MF (2006) Two-level antibacterial coating with both release-killing and contact-killing capabilities. Langmuir 22(24):9820–9823
13. Shekhar A, Soumyo M, Suparna MJN (2013) Immobilized silver nanoparticles enhance contact killing and show highest efficacy: elucidation of the mechanism of bactericidal action of silver. Nanoscale 5(16):7328–7340
14. Deng L, Deng Y, Xie K (2017) AgNPs-decorated 3D printed PEEK implant for infection control and bone repair. Colloids Surf B Biointerfaces 160:483–492
15. Stelzig SH, Menneking C, Hoffmann MS, Eisele K, Barcikowski S, Klapper M, Müllen KJEPJ (2011) Compatibilization of laser generated antibacterial Ag-and Cu-nanoparticles for perfluorinated implant materials. Eur Polym J 47(4):662–667
16. Bai H, Yuan H, Nie C, Wang B, Lv F, Liu L, Wang S (2015) A supramolecular antibiotic switch for antibacterial regulation. Angew Chem Int Ed 54(45):13208–13213
17. Walsh C (2000) Molecular mechanisms that confer antibacterial drug resistance. Nature 406(6797):775–781
18. Gold HS, Moellering RC Jr (1996) Antimicrobial-drug resistance. N Engl J Med 335(19):1445–1453
19. Stewart PS, Costerton JW (2001) Antibiotic resistance of bacteria in biofilms. Lancet 358(9276):135–138
20. Chandra J, Kuhn DM, Mukherjee PK, Hoyer LL, McCormick T, Ghannoum MA (2001) Biofilm formation by the fungal pathogen Candida albicans: development, architecture, and drug resistance. J Bacteriol 183(18):5385–5394
21. Coad BR, Kidd SE, Ellis DH, Griesser HJ (2014) Biomaterials surfaces capable of resisting fungal attachment and biofilm formation. Biotechnol Adv 32(2):296–307
22. Poverenov E, Shemesh M, Gulino A, Cristaldi DA, Zakin V, Yefremov T, Granit R (2013) Durable contact active antimicrobial materials formed by a one-step covalent modification of polyvinyl alcohol, cellulose and glass surfaces. Colloids Surf B Biointerfaces 112:356–361
23. Windler L, Height M, Nowack B (2013) Comparative evaluation of antimicrobials for textile applications. Environ Int 53:62–73
24. Bandyopadhyay D, Prashar D, Luk Y-Y (2011) Anti-fouling chemistry of chiral monolayers: enhancing biofilm resistance on racemic surface. Langmuir 27(10):6124–6131

25. Fu Q, Zhang K, Gao D, Wang L, Yang F, Liu Y, Xia Z (2017) Escherichia coli adhesive coating as a chiral stationary phase for open tubular capillary electrochromatography enantioseparation. Anal Chim Acta 969:63–71
26. Shi B, Luan D, Wang S, Zhao L, Tao L, Yuan Q, Wang X (2015) Borneol-grafted cellulose for antifungal adhesion and fungal growth inhibition. RSC Adv 5(64):51947–51952
27. Luo L, Li G, Luan D, Yuan Q, Wei Y, Wang X (2014) Antibacterial adhesion of borneol-based polymer via surface chiral stereochemistry. ACS Appl Mater Interfaces 6(21):19371–19377
28. Hanein D, Sabanay H, Addadi L, Geiger B (1993) Selective interactions of cells with crystal surfaces. Implications for the mechanism of cell adhesion. J Cell Sci 104(2):275–288
29. Hanein D, Geiger B, Addadi L (1994) Differential adhesion of cells to enantiomorphous crystal surfaces. Science 263(5152):1413–1416
30. Sun T, Han D, Rhemann K, Chi L, Fuchs H (2007) Stereospecific interaction between immune cells and chiral surfaces. J Am Chem Soc 129(6):1496–1497
31. Bandyopadhyay D, Prashar D, Luk Y-Y (2011) Stereochemical effects of chiral monolayers on enhancing the resistance to mammalian cell adhesion. Chem Commun 47(21):6165–6167
32. Ayres N (2010) Polymer brushes: Applications in biomaterials and nanotechnology. Polym Chem 1(6):769–777
33. Wang X, Gan H, Zhang M, Sun T (2012) Modulating cell behaviors on chiral polymer brush films with different hydrophobic side groups. Langmuir 28(5):2791–2798
34. Wang X, Gan H, Sun T, Su B, Fuchs H, Vestweber D, Butz S (2010) Stereochemistry triggered differential cell behaviours on chiral polymer surfaces. Soft Matter 6(16):3851–3855
35. Liu G, Zhang D, Feng C (2014) Control of three-dimensional cell adhesion by the chirality of nanofibers in hydrogels. Angew Chem Int Ed 53(30):7789–7793
36. Liu J, Yuan F, Ma X, Auphedeous D i Y, Zhao C, Liu C, Shen C, Feng C (2018) The cooperative effect of both molecular and supramolecular chirality on cell adhesion. Angew Chem Int Ed 130(22):6585–6589
37. Li Y, Zhou Y, Wang HY, Perrett S, Zhao Y, Tang Z, Nie G (2011) Chirality of glutathione surface coating affects the cytotoxicity of quantum dots. Angew Chem Int Ed 50(26):5860–5864
38. Deng J, Wu S, Yao M, Gao C (2016) Surface-anchored poly(acryloyl-L (D)-valine) with enhanced chirality-selective effect on cellular uptake of gold nanoparticles. Sci Rep 6:31595
39. Kehr NS, Jose J (2017) Chirality-dependent cellular uptake of chiral nanocarriers and intracellular delivery of different amounts of guest molecules. Appl Surf Sci 425:432–439
40. El-Gindi J, Benson K, De Cola L, Galla HJ, Seda Kehr N (2012) Cell adhesion behavior on enantiomerically functionalized zeolite L monolayers. Angew Chem Int Ed 51(15):3716–3720
41. Wang X, Gan H, Sun T (2011) Chiral design for polymeric biointerface: the influence of surface chirality on protein adsorption. Adv Funct Mater 21(17):3276–3281
42. Wang X, Wang M, Lei R, Zhu SF, Zhao Y, Chen C (2017) Chiral surface of nanoparticles determines the orientation of adsorbed transferrin and its interaction with receptors. ACS Nano 11(5):4606–4616
43. Wang X, Wang X, Wang M, Zhang D, Yang Q, Liu T, Lei R, Zhu S, Zhao Y, Chen C (2018) Probing adsorption behaviors of BSA onto chiral surfaces of nanoparticles. Small 14(16):1703982
44. Gao G, Zhang M, Lu P, Guo G, Wang D, Sun T (2015) Chirality-assisted ring-like aggregation of Aβ(1-40) at liquid-solid interfaces: a stereoselective two-step assembly process. Angew Chem Int Ed 54(7):2245–2250
45. Qing G, Zhao S, Xiong Y, Lv Z, Jiang F, Liu Y, Chen H, Zhang M, Sun T (2014) Chiral effect at protein/graphene interface: a bioinspired perspective to understand amyloid formation. J Am Chem Soc 136(30):10736–10742
46. Deng J, Li Z, Yao M, Gao C (2016) Influence of albumin configuration by the chiral polymer-grafted gold nanoparticles. Langmuir 32(22):5608–5616
47. Zhou F, Yuan L, Li D, Huang H, Sun T, Chen H (2012) Cell adhesion on chiral surface: the role of protein adsorption. Colloids Surf B Biointerfaces 90:97–101
48. Tang K, Gan H, Li Y, Chi L, Sun T, Fuchs H (2008) Stereoselective interaction between DNA and chiral surfaces. J Am Chem Soc 130(34):11284–11285

49. Gan H, Tang K, Sun T, Hirtz M, Li Y, Chi L, Butz S, Fuchs H (2009) Selective adsorption of DNA on chiral surfaces: supercoiled or relaxed conformation. Angew Chem Int Ed 48(29):5282–5286
50. Sun X, Qian Z, Luo L, Yuan Q, Guo X, Lei T, Wei Y, Xing W (2016) Antibacterial adhesion of polymethyl methacrylate modified by borneol acrylate. ACS Appl Mater Interfaces 8(42):28522–28528
51. Xu J, Bai Y, Wan M, Liu Y, Tao L, Wang X (2018) Antifungal paper based on a polyborneolacrylate coating. Polymers 10(4):448
52. Wang X, Jing S, Liu Y, Liu S, Tan Y (2017) Diblock copolymer containing bioinspired borneol and dopamine moieties: synthesis and antibacterial coating applications. Polymer 116:314–323
53. Wu J, Wang C, Mu C, Lin W (2018) A waterborne polyurethane coating functionalized by isobornyl with enhanced antibacterial adhesion and hydrophobic property. Eur Polym J 108:498–506
54. Krizova H, Wiener J (2013) Development of carboxymethyl cellulose/polyphenols gels for textile applications. Autex Res J 13(2):33–36
55. Tankhiwale R, Bajpai S (2009) Graft copolymerization onto cellulose-based filter paper and its further development as silver nanoparticles loaded antibacterial food-packaging material. Colloids Surf B Biointerfaces 69(2):164–168
56. Gemili S, Yemenicioğlu A, Altınkaya SA (2009) Development of cellulose acetate based antimicrobial food packaging materials for controlled release of lysozyme. J Food Eng 90(4):453–462
57. Petersen N, Gatenholm P (2011) Bacterial cellulose-based materials and medical devices: current state and perspectives. Appl Microbiol Biotechnol 91(5):1277
58. Cherian BM, Leão AL, de Souza SF, Costa LMM, de Olyveira GM, Kottaisamy M, Nagarajan E, Thomas S (2011) Cellulose nanocomposites with nanofibres isolated from pineapple leaf fibers for medical applications. Carbohydr Polym 86(4):1790–1798
59. Dautzenberg H, Schuldt U, Grasnick G, Karle P, MÜller P, LÖhr M, Pelegrin M, Piechaczyk M, Rombs KV, GÜnzburg WH (1999) Development of cellulose sulfate-based polyelectrolyte complex microcapsules for medical applications. Ann N Y Acad Sci 875(1):46–63
60. Ude S, Arnold DL, Moon CD, Timms-Wilson T, Spiers AJ (2006) Biofilm formation and cellulose expression among diverse environmental Pseudomonas isolates. Environ Microbiol 8(11):1997–2011
61. Feese E, Sadeghifar H, Gracz HS, Argyropoulos DS, Ghiladi RA (2011) Photobactericidal porphyrin-cellulose nanocrystals: synthesis, characterization, and antimicrobial properties. Biomacromolecules 12(10):3528–3539
62. Xu J, Zhao H, Xie Z, Ruppel S, Zhou X, Chen S, Liang JF, Wang X (2019) Stereochemical strategy advances microbially antiadhesive cotton textile in safeguarding skin flora. Adv Healthc Mater 8(12):1900232
63. Kumar MNR (2000) A review of chitin and chitosan applications. React Funct Polym 46(1):1–27
64. Rinaudo M (2006) Chitin and chitosan: properties and applications. Prog Polym Sci 31(7):603–632
65. Elsabee MZ, Abdou ES (2013) Chitosan based edible films and coatings: a review. Mater Sci Eng C 33(4):1819–1841
66. Ilium L (1998) Chitosan and its use as a pharmaceutical excipient. Pharm Res 15(9):1326–1331
67. Kumar MR, Muzzarelli RA, Muzzarelli C, Sashiwa H, Domb A (2004) Chitosan chemistry and pharmaceutical perspectives. Chem Rev 104(12):6017–6084
68. Fu YN, Li Y, Li G, Yang L, Yuan Q, Tao L, Wang X (2017) Adaptive chitosan hollow microspheres as efficient drug carrier. Biomacromolecules 18(7):2195–2204
69. Shahidi F, Arachchi JKV, Jeon Y-J (1999) Food applications of chitin and chitosans. Trends Food Sci Technol 10(2):37–51
70. Wang H, Qian J, Ding F (2018) Emerging chitosan-based films for food packaging applications. J Agric Food Chem 66(2):395–413

71. Naz F, Zuber M, Zia KM, Salman M, Chakraborty J, Nath I, Verpoort F (2018) Synthesis and characterization of chitosan-based waterborne polyurethane for textile finishes. Carbohydr Polym 200:54–62
72. Dutta P, Tripathi S, Mehrotra G, Dutta J (2009) Perspectives for chitosan based antimicrobial films in food applications. Food Chem 114(4):1173–1182
73. Lang G, Clausen T (1989) The use of chitosan in cosmetics. Chitin and chitosan. Sources, Chemistry, Biochemistry. Physical Properties and Applications, vol 139. Elsevier Applied Science, London and New York, p 147
74. Jimtaisong A, Saewan N (2014) Utilization of carboxymethyl chitosan in cosmetics. Int J Cosmet Sci 36(1):12–21
75. Liu N, Chen X-G, Park H-J, Liu C-G, Liu C-S, Meng X-H, Yu L-J (2006) Effect of MW and concentration of chitosan on antibacterial activity of Escherichia coli. Carbohydr Polym 64(1):60–65
76. Sudarshan N, Hoover D, Knorr D (1992) Antibacterial action of chitosan. Food Biotechnol 6(3):257–272
77. Kong M, Chen XG, Xing K, Park HJ (2010) Antimicrobial properties of chitosan and mode of action: a state of the art review. Int J Food Microbiol 144(1):51–63
78. Vaz JM, Pezzoli D, Chevallier P, Campelo CS, Candiani G, Mantovani D (2018) Antibacterial coatings based on chitosan for pharmaceutical and biomedical applications. Curr Pharm Des 24(8):866–885
79. Foster LJR, Butt J (2011) Chitosan films are NOT antimicrobial. Biotechnol Lett 33(2):417–421
80. Pinto RJ, Fernandes SC, Freire CS, Sadocco P, Causio J, Neto CP, Trindade T (2012) Antibacterial activity of optically transparent nanocomposite films based on chitosan or its derivatives and silver nanoparticles. Carbohydr Res 348:77–83
81. Fu J, Ji J, Fan D, Shen J (2006) Construction of antibacterial multilayer films containing nanosilver via layer-by-layer assembly of heparin and chitosan-silver ions complex. J Biomed Mater Res A 79(3):665–674
82. Jia Z, Xu W (2001) Synthesis and antibacterial activities of quaternary ammonium salt of chitosan. Carbohydr Res 333(1):1–6
83. Vallapa N, Wiarachai O, Thongchul N, Pan J, Tangpasuthadol V, Kiatkamjornwong S, Hoven VP (2011) Enhancing antibacterial activity of chitosan surface by heterogeneous quaternization. Carbohydr Polym 83(2):868–875
84. Costa F, Carvalho IF, Montelaro RC, Gomes P, Martins MCL (2011) Covalent immobilization of antimicrobial peptides (AMPs) onto biomaterial surfaces. Acta Biomater 7(4):1431–1440
85. Xin Y, Zhao H, Xu J, Xie Z, Li G, Gan Z, Wang X (2019) Borneol-modified chitosan: antimicrobial adhesion properties and application in skin flora protection. Carbohydr Polym 228:115378
86. Hegab HM, Elmekawy A, Zou L, Mulcahy D, Saint CP, Ginic-Markovic M (2016) The controversial antibacterial activity of graphene-based materials. Carbon 105:362–376
87. Zou X, Zhang L, Wang Z, Luo Y (2016) Mechanisms of the antimicrobial activities of graphene materials. J Am Chem Soc 138(7):2064–2077
88. Zhu J, Wang J, Hou J, Zhang Y, Liu J, Bruggen BV (2017) Graphene-based antimicrobial polymeric membranes: a review. J Mater Chem A 5(15):6776–6793
89. Li G, Zhao H, Hong J, Quan K, Yuan Q, Wang X (2017) Antifungal graphene oxide-borneol composite. Colloids Surf B Biointerfaces 160:220–227
90. Dai X, Guo Q, Zhao Y, Zhang P, Zhang T, Zhang X, Li C (2016) Functional silver nanoparticle as a benign antimicrobial agent that eradicates antibiotic-resistant bacteria and promotes wound healing. ACS Appl Mater Interfaces 8(39):25798–25807
91. Jia Z, Shi Y, Xiong P, Zhou W, Cheng Y, Zheng Y, Xi T, Wei S (2016) From solution to biointerface: graphene self-assemblies of varying lateral sizes and surface properties for biofilm control and osteo-differentiation. ACS Appl Mater Interfaces 8(27):17151–17165
92. Li G, Quan K, Xu C, Deng B, Wang X (2018) Synergy in thrombin-graphene sponge for improved hemostatic efficacy and facile utilization. Colloids Surf B Biointerfaces 161:27–34

93. Motealleh A, Hermes H, Jose J, Kehr NS (2018) Chirality-dependent cell adhesion and enrichment in Janus nanocomposite hydrogels. Nanomed Nanotechnol Biol Med 14(2):247–256
94. Guo Y, Yao R, Wang Z, Zhang Y, Cui M, Zhao Q, Wang H (2018) Novel potential type electrochemical chiral recognition biosensor for amino acid. J Solid State Electrochem 22(1):41–49
95. Feng L, Xu B, Ren J, Zhao C, Qu X (2012) A human telomeric DNA-based chiral biosensor. Chem Commun 48(72):9068–9070
96. Bommarius AS, Schwarm M, Drauz K (1998) Biocatalysis to amino acid-based chiral pharmaceuticals—examples and perspectives. J Mol Catal B: Enzym 5(1-4):1–11
97. Wistuba D, Schurig V (2000) Enantiomer separation of chiral pharmaceuticals by capillary electrochromatography. J Chromatogr A 875(1-2):255–276
98. Evans SE, Davies P, Lubben A, Kasprzyk-Hordern B (2015) Determination of chiral pharmaceuticals and illicit drugs in wastewater and sludge using microwave assisted extraction, solid-phase extraction and chiral liquid chromatography coupled with tandem mass spectrometry. Anal Chim Acta 882:112–126